Uniform Tilt-Angle Micromirror Array for Multi Object Spectroscopy

Severin Waldis[a], Pierre-Andre Clerc[a], Frederic Zamkotsian[b], Michael Zickar[a], Wilfried Noell[a], Nico de Rooij[a]

[a]IMT, University of Neuchatel, Jaquet Droz 1, CH-2007 Neuchatel, Switzerland
[b]Laboratoire d'Astrophysique de Marseille, 2 place Leverrier, F-13248 Marseille Cedex 4, France

ABSTRACT

We report on micromirror arrays being developed for the use as reflective slit mask in Multi Object Spectrographs for astronomical applications. The micromirrors are etched in bulk single crystal silicon whereas the cantilever type suspension is realized by surface micromachining. One micromirror element is 100μm x 200μm in size. The micromirrors are actuated electrostatically by electrodes located on a second chip. The use of silicon on insulator (SOI) wafers for both mirror and electrode chip ensures thermal compatibility for cryogenic operation. A system of multiple landing beams has been developed, which passively locks the mirror at a well defined tilt angle when actuated. The mechanical tilt angle obtained is 20° at a pull-in voltage of 90V. Measurements with an optical profiler showed that the tilt angle of the actuated and locked mirror is stable with a precision of one arc minute over a range of 15V. This locking system makes the tilt angle merely independent from process variations across the wafer and thus provides uniform tilt angle over the whole array. The precision on tilt angle from mirror to mirror measured is one arc minute. The surface quality of the mirrors in actuated state is better than 10nm peak-to-valley and the local roughness is around 1nm RMS.

Keywords: micromirror, multi object spectroscopy, MOEMS, mirror array, DRIE

1. INTRODUCTION

Thanks to its multiplexing capabilities, Multi-Object Spectroscopy (MOS) is becoming the central method to study large numbers of objects in astronomical fields, recording simultaneously hundreds of spectra. For one of the most central astronomical program, deep spectroscopic survey of galaxies, the density of objects is low and it is necessary to probe wide fields of view. The objects of interest have to be selected (whatever the criteria distance, color, magnitude, etc.) within deep spectroscopic surveys. This saves time and therefore increases the scientific efficiency of observations.

These remote sources spectra are strongly shifted toward higher wavelengths due to the expansion of the Universe (Doppler effect), this is the so-called red-shift effect. Then the spectrographs have to work in the infra-red wavelengths, and, in order to avoid the emission of the "warm" elements at these wavelengths, the instrument must be able to work at cryogenic temperature inside cryostats for ground-based instruments or in the space environment for space telescopes.

Future generation of Near Infra-Red MOS is already under study for Extremely Large Telescopes (ELT) and future space telescopes. The most advanced project is the Near Infrared Multi-Object Spectrograph (NIRSpec) for the James Webb Space Telescope (JWST). The James Webb Space Telescope (JSWT), a next generation space telescope developed by NASA, ESA and CSA in order to replace the 2.4m Hubble Space Telescope, has a diameter of 6.5m and is scheduled to be launched in 2013. This telescope will work in the 0.6μm to 28μm wavelength band. It will be located at the Lagrange point L2 for a passive cooling down to 35K. In order to

Further author information:
S.W.: E-mail: severin.waldis@unine.ch, Telephone: +41 32 720 55 71
F.Z.: E-mail: frederic.zamkotsian@oamp.fr, Telephone: + 33 4 95 04 41 51

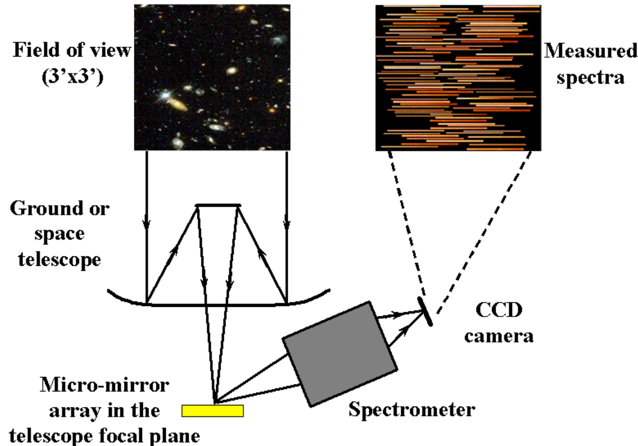

Figure 1. Principle of a Multi-Object Spectrograph with a Micro-Mirror Array. Objects are selected of an astronomical field of view and spectra are obtained on the spectrograph detector.

obtain spectra of hundreds of objects simultaneously, the NIRSpec for JWST requires a reconfigurable multi-slit device (MSD). Conventional masks or complex fiber-optics-based mechanisms are impracticable in space, where an MSD requires remote control of the multi-slit configuration. Micro-optical components based on the micro-electronics fabrication process, the so called micro-optical-electro-mechanical systems (MOEMS) have been chosen for NIRSpec. MOEMS have produced a wide range of applications, like sensors, switches, micro-shutters, beam deflectors and micro-deformable mirrors. A promising solution is the use of a micro-mirror array (MMA) for generating reflecting slits[1,2] or a micro-shutter array (MSA) for generating transmissive slits.[3]

By placing the programmable slit mask in the focal plane of the telescope, the light from selected objects is directed toward the spectrograph (ON state), while the light from others objects and from the sky background is blocked (OFF state). Fig. 1 shows the MEMS based MOS concept, with a MMA as programmable slit mask. Using a MMA, any required slit configuration might be obtained with the capability to match point sources or extended objects. Also, the MMA enables the use of the so called "long slit" mode, which Astronomers use often with the classical slit mask. In long slit mode a longer slit than the actual size of the studied objects is generated. This is used for the simultaneous recording of the spectrum of the object and the nearby spectrum of the background; by subtracting the background spectrum , the pure spectrum of the object is finally obtained. A possible MMA candidate would be the DMD device from TI, but this component is not suited for astronomical MOS due to the small size of the micromirrors and the impossibility to work at cryogenic temperatures.

OPTICON is the network gathering the research efforts of the European astronomical community; a Joint Research Activity (JRA) has been set on Smart Focal Planes for developing components to be used in the focal plane of the telescope for selecting or re-arranging the light of the astronomical objects. Within the framework of this JRA, micro-mirrors have been selected in order to get a first demonstrator of a European MOEMS-based slit mask.

We present in this paper the basic concept of the developed device, its analytical modeling as well as finite element method simulation and the realization. Finally we report on the optical and electromechanical characterization of the first generation devices.

2. CONCEPT

We have developed over several years different tools for the modeling and the characterization of these MOEMS-based slit masks, during the design studies on JWST-NIRSpec. The models, based on Fourier theory, address two key parameters for the MOS performance: spectral photometric variation (SPV) and contrast. The SPV is the unpredictable photometric variation due to the random repartition of the sources on the slit mask. The SPV

requirement is generally $< 10\%$, but as SPV is strongly dependent on the object position and wavelength, the required value cannot be reached. A dithering strategy has been proposed for solving this problem.[4] Contrast is defined as the total amount of non-selected flux of light passing through the multi-slit device when the device is set in the OFF position, compared to the amount of light passing in the ON position. To avoid spoiler sources (bright stars or galaxies within the instrument field of view) and background to pollute spectra, its value has to be as high as possible. According to the density of objects (stars and galaxies) in the field of view and their magnitude, a contrast requirement of 3000:1 has been established. A characterization bench has also been developed for the measurement of these parameters.[5]

Based on our simulations and measurements, we have fixed several parameters: In a first approach we set one micromirror per astronomical object, which corresponds to the baseline for NIRSpec. It is essential for this instrument to achieve a high optical contrast of at least 3000:1. The tilted micromirror is used for the ON position and the rest position is considered as OFF. Hence the amount of parasitic light can be drastically minimized that comes from reflections and scattering of the frame surrounding the micromirrors and of the underneath electrodes. A useable mechanical tilting angle must exceed 20°. The mirror surface must remain flat in operation throughout a large temperature range. The fill factor of more than 90% is essential, at least along the long slit. One micromirror element has to be at least 100μm x 200μm, in order to correspond with the plate scale of 8m-class telescopes as well as future extremely large telescopes (ELT's). The micromirror array has to work at cryogenic temperatures.

The basic concept of the device is shown in Figure 2. The MOS micromirrors are actuated electrostatically. Thermal actuation is not suited for infrared applications, piezo-electric actuation is not suited due to its small stroke and magnetic actuation is very complex on system level.[3] The electrostatic actuation combines the required low power dissipation, high stroke and simplicity on system level. As the device is used as object selector, it is operated in binary mode, i.e. there is a OFF and a ON state. The flat, non-actuated state of the mirrors (shown in Fig. 2 (a)) is considered as the OFF state, both mirror and electrode are grounded. The pull-in state of the mirror, precisely when the mirror is tilted as shown in Fig. 2 (d) is considered as the ON state.

A single cell of the device consists of a mirror, which is suspended to a supporting frame by a flexible beam, an electrode and a spacer element that provides a constant gap between mirror and electrode. In the two-dimensional arrays the frame is designed to run along only the long side of the mirror, which makes near 100% fill-factor possible along this direction. Stopper beams located on the mirror and the frame provide tilt angle control. Physically, the device is realized on two different chips: the mirror chip and the electrode chip. The latter contains the spacer elements.

In order to have mirrors with a planarity better than $\lambda/20$, thick mirrors are used. With a mirror size of 100μm x 200μm, a thickness of 10μm is supposed to be sufficient in order to keep the mirror flat during actuation. The flexion hinge type suspension is situated on the backside of the mirror. This hidden suspension beam configuration leads to a higher fill-factor than lateral suspension beams. In addition, as the suspension is covered by the mirror (except for the small gap between mirror and frame), we have no stray light coming from the bent beams, which means less degradation of the contrast. The contrast value depends upon the tilt-angle of the mirror, that is the angle between the OFF and the ON state of one mirror. The degradation of the contrast is usually due to the stray light originating from the mirror edges, supporting frame, suspension and backscattered light from the electrode. As the suspension is hidden by the mirror and the gap-size between mirror and frame is small, the degradation of the contrast is mainly due to the rounding of the mirror edges, surface roughness of the mirror and of the frame. The tilt angle is a function of the gap between the electrode and the mirror and the geometry of the suspension. With a intended gap height of 35 μm, tilting angles between 15° and 24° can be achieved. A tilt angle of 20° should yield a contrast better than 3000:1. A system of landing posts (or stopper beams) on the mirror and on the frame has been developed to assure a precise and constant tilt-angle. This concept is shown in Fig. 2: Once the mirror (i.e. the landing post located on the mirror) touches the electrode, it will not stop moving but start to turn into the opposite direction around this new rotation axis. That is, the tilting angle tends to decrease once the mirror has landed. This is due to a non-zero (and opposite to the mirror tilting motion) torque around the point where the landing post is attached to the mirror. The reverse turning movement is stopped at a well-defined tilt-angle by the stopper beam attached to the frame adjacent the mirror.

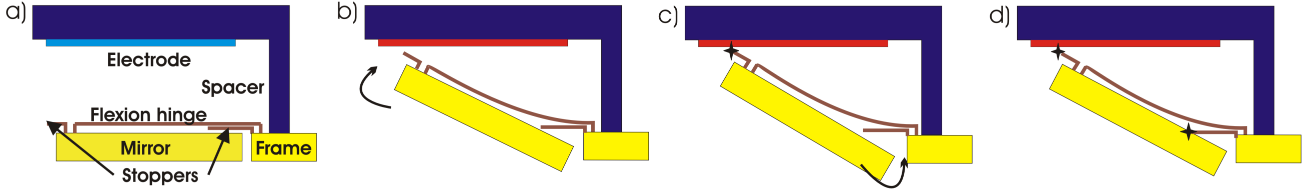

Figure 2. Schematic view of the basic concept (a) and the electrostatic latching mechanism used to achieve stable tilt angles: Due to the electrostatic force the mirror rotates upwards (b) until the first stopper beam, which is attached to the mirror, hits the electrode (c). Then the mirror starts rotating in the inverse direction until it hits the second stopper beam, which is attached to the mirror frame (d), and remains electrostatically fixed in this position.

The mirror is now electrostatically latched in a position defined by the geometry of the landing posts and the gap between electrode and mirror.

The mirror and electrode chip are fabricated separately on different wafers and assembled afterward. The mirror chip is made out of a silicon on insulator (SOI) wafer. The 10μm thick silicon on insulator layer (or, device layer) is structured into (horizontal) mirrors and frame by bulk micromachining. The optical active side of the mirror is the backside of the device layer, which must be released during fabrication. Intrinsically the device layer backside is optically flat in terms of roughness and, when released, optical flat in terms of planarity (better than $\lambda/20$) over a rectangle of 100μm x 200μm. The suspension structure and the landing posts are realized by surface micromachining of a deposited and doped polycrystalline silicon layer underneath the mirror and frame. Poly-silicon is used rather than another material as it has a thermal expansion coefficient similar to single crystal silicon. This is important for the operation in cryogenic environment. In order to assure the thermal expansion compatibility with the mirror chip, the electrode chip is also based on a SOI silicon wafer. Beside the electrodes, connecting lines and connecting pads, the electrode chip also contains the spacer elements, which ensure a constant gap between the electrode and the mirror chip. The spacer height is fixed and defined by the thickness of the device layer of the electrode chip, therefore the uniformity of the spacer height (and the uniformity of tilt-angle) depends on the uniformity in thickness of this silicon layer. The effective gap height can be tuned during the etching of the electrode.

3. MODELING

The required mechanical tilt angle of the MOS micromirrors is 20°. For this given tilt angle we want to minimize the required gap height, i.e. the spacing between the mirror and the electrode. This for the following reasons:

1. For a given geometry of the flexure beam, the actuation voltage is proportional to the gap height.
2. The present actuator architecture implies that a part of the tilted mirror (ON state) is optically blocked from the adjacent frame. This covering reduces the operational fill factor. It can be minimized by minimizing the gap height.
3. The crosstalk between two adjacent mirror depends upon the gap height, the smaller the gap height, the less pronounced the cross talk.

In this section we discuss the effects of the suspension and stopper geometry and electrode position on the behavior of the actuator.

The dimensions of the flexion beams are determined by the constraint on the resonance frequency, actuation voltage and the maximum allowable stress. The only degrees of freedom to influence the tilt angle per gap height ratio are the suspension attachment offset (parameter b in Fig. 3) and the relative position of the electrode (parameter e in Fig. 3).

We consider the case of a cantilever suspension as shown in Fig. 3. Assuming a thin (i.e. width $\gg$ thickness) cantilever we can neglect the in-plane movement of the mirror and can consider only the movement in the plane perpendicular to the mirror. Furthermore if we consider that the mirror is much thicker and larger than the

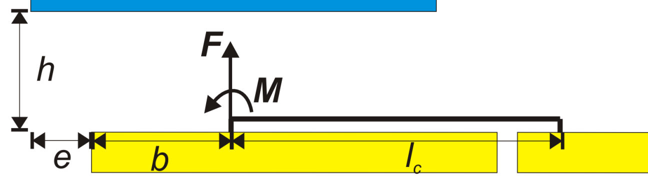

Figure 3. Suspension model. The electrostatic forces acting on the mirror are replaced by a resulting force and moment acting on the endpoint of the suspension cantilever.

cantilever, we can assume the mirror to be rigid*. The electrostatic forces acting on the mirror can then be reduced to a resulting force and moment acting on the point where the cantilever is attached to the mirror, as shown in Fig. 3. The resulting piston movement and tilt angle due to the force F and the moment M is obtained by linear superposition, i.e. summation of the two individual contributions. Considering small deflections we can write for the y-deflection of the cantilevers end

$$\begin{aligned} \delta &= \delta_F - \delta_M \\ &= \frac{l_c^2}{EI_y}\left(\frac{Fl_c}{3} - \frac{M}{2}\right) \end{aligned} \tag{1}$$

and for the angle

$$\begin{aligned} \alpha &= \alpha_F - \alpha_M \\ &= \frac{l_c}{EI_y}\left(\frac{Fl_c}{2} - M\right) \end{aligned} \tag{2}$$

where l_c is the cantilever length, E Young's modulus and I_y the moment of inertia around the y-axis.[6] The moment of inertia is given with $I_y = wd^3/12$, where w is the width of the cantilever and d the thickness. Eq. 1 represents the (vertical) piston movement of the mirror and Eq. 2 the tilt angle. Note that the ratio α/δ (obtained from Eqs. 1-2) decreases with the length of the cantilever l_c. It is obvious from Eq. 2 that for a mirror motion as shown in Fig. 2 (b), we must have $Fl_c > 2 * M$. If we have $Fl_c < 2 * M$ the mirror tilts in the opposite direction. The relation between F and M depends on the suspension attachment offset b and the relative position of the electrode to the mirror e. Consider now $b = 0$ and the electrostatic pressure on the mirror as p_E where the electrode covers the mirror and 0 otherwise. We can then write for the resulting moment

$$M = p_E \frac{(l_m - e)^2}{2} \tag{3}$$

and for the resulting force

$$F = p_E(l_m - e) \tag{4}$$

It follows immediately that for $l_m = l_c$ and $e = 0$ the angle α is zero. Thus we need an asymmetry either in the electrode positioning or flexion beam geometry for optimum performance of the device. The optimum positioning of the electrode depends on the positioning of the flexion beam. Considering now $e = 0$ and $b \neq 0$. Writing the electrostatic pressure as $p = F/l_m$ the resulting resulting force would then be F and the resulting moment

$$\begin{aligned} M &= \int_{-b}^{0} \frac{F}{l_m} x dx + \int_{0}^{l_m} \frac{F}{l_m} x dx \\ &= \frac{l - 2b}{2} F \end{aligned} \tag{5}$$

*The deflection δ due to a force F of a beam with rectangular section wh can be written as $\delta \sim F/wh^3$. Assuming a beam with 10x0.5 μm section and a mirror with a 200x10 μm section, having the same length, a force F would deflect the mirror $20^4 = 160000$ times less than the cantilever.

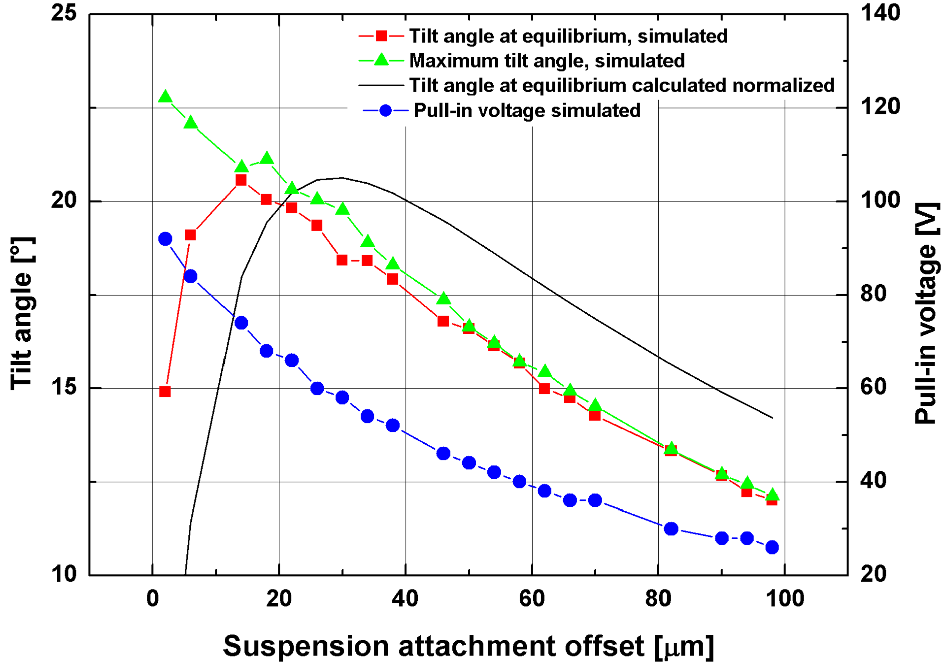

Figure 4. Tilt angle and pull-in voltage versus suspension offset b for a gap height $h = 35\mu$m and flexion beam dimensions $d = 0.5\mu$m, $w = 10\mu$m and $l_c = 100\mu$m. As comparison, a normalized plot of the analytic formula for the pull-in voltage is drawn (dashed curve)

By combining equations 1- 5, we can predict the mirror angle and piston in function of the cantilever attachment offset b. For small angles the gap height equals $\delta + b\alpha$. Putting $l_m = l_c = l$ we can write for the tilt angle versus gap height ratio

$$\frac{\alpha}{\delta + \alpha b} = \frac{b}{b^2 + \frac{l}{2}b + \frac{l^2}{12}} \tag{6}$$

The normalized function is plotted in graph 4. We note a strong dependence of the tilt angle per gap height ratio on the positioning of the flexion beam attachment point. The maximum value occurs at $b = l/\sqrt{12}$.

Considering the real case, where large deflections and large angles occur, simulations using the finite element method (FEM) must be carried out. Large out-of-plane movements, especially tilting movements, often cause convergence problems in coupled electrostatic and mechanical simulation due to strong mesh deformation and non-linearities. Non-linearities occur due to stress-stiffening, which must be taken into account when considering large deflections of the cantilever and can not be avoided. Mesh-deformation can be avoided by re-meshing the electrostatic and mechanical model after each iteration. Thus we developed a script-based custom 2D electro-mechanical model for the use with ANSYS. The principal idea is to separate the mechanical and electrostatic model. The electrostatic model calculates the forces that act on the mirror; the resulting force and moment is then transferred onto the cantilever in the mechanical model. The simulation of the mechanical model gives then the deflection of the cantilever and the new position of the mirror, which is again transferred into the electrostatic model. For each iteration the electrostatic model is rebuild and re-meshed based on the geometrical data calculated by the mechanical (cantilever) model. Simulations where carried out varying the key-parameters of the micromirror device: cantilever geometry, cantilever position, electrode position and gap height. Tilt angle, pull-in voltage, maximum stress and the first resonance frequency were extracted from the simulations. The first resonance frequency, which is a measure for shock resistivity, is between 800Hz and 2kHz for different designs, which is an acceptable range for the considered application. The maximum stress in the cantilever, ranges from 120MPa to 400MPa, designs which exceeds 400MPa are not considered. Based on this simulations we set the dimensions of the cantilever to be 70μm - 100μm in length, 0.3 μm - 0.6 μm in thickness and 3μm - 7μm in

width. The gap height is set to 35μm.

For studying the influence of the electrode position and the cantilever attachment point on the tilt angle per gap height ratio we fixed the gap height and searched the highest tilt angle for this given gap. This comes to the same as minimizing the gap height for a given tilt angle, because, as simulation confirmed, the tilt angle goes linear with the gap height for a given configuration. We found that indeed there is a maximum tilt angle in function of the positioning of the electrode (parameter e), albeit it is not very pronounced. The position of the maximum depends upon the cantilever attachment offset b, for increasing b, e decreases. We set $e = l_m/10$, which corresponds to the ideal position for $b = l_m/5$.

The dependency of the tilt angle (for a given gap and a given electrode offset) is shown in Fig. 4. Consider first the tilt angle at equilibrium, that is the position where the mirror is in steady state, at the indicated pull-in voltage and without the stopper beam system. Note that the simulated curve has the same shape as the calculated curve but its maximum is shifted. This is due to the shifted electrode ($e = l_m/10$) used for the simulation. If we look at the evolution of the tilt angle rather than the steady state, we note that the tilt angle reaches a maximum value, before the mirror is settled in the steady state. This result confirms the hypothesys made for the latching system showed in Fig. 2 (c): Once the mirror hit the electrode, it starts to rotate in the inverse direction, decreasing its tilt angle. In order to have the mirror latched as proposed in Fig. 2 (d), the geometry of the stopper beams must be chosen such that they stop the mirror between the maximum and the equilibrium tilt angle. The range between the maximum and the steady state value can be considered as the tuning range of the tilt angle for a given gap height. One could, by augmenting the actuation voltage beyond the pull-in voltage, extend this range, i.e. lower the steady state value. However, this is not suited for our application as we intend to use a hold voltage lower than the pull-in voltage. Ideally, the stopper beams are adjusted such that the mirror is stopped shortly after reaching the maximum tilt angle. This way the useable range for the hold voltage is maximized. We remark that the difference between the maximum and the steady state tilt angle decreases strongly with increasing b. The absolute value of the maximum achievable tilt angle, also decreases with increasing b. Thus for a maximum tilt angle per gap height ratio and for a maximum tuning range we chose $0\mu m \leq b \leq 20\mu m$. The geometry, i.e. the length, of the stopper beams is chosen such that the mirror is stopped at an angle 10% of the tuning range below the maximum value. This margin accounts for process variations. That way the proper function of the latching mechanism and thus the uniform tilt angle is assured. The uniform tilt angle condition is a crucial requirement for the mirror array to be used in a MOS system.

4. REALIZATION

Arrays of 2x2 and 5x5, as well as single mirrors with either flexion or torsion beam suspension and different types of electrodes have been fabricated. Mirror sizes of 100μm x 200μm, 200μm x 100μm and 250μm x 500μm have been implemented. Flexion and torsion beams with various lengths and widths and a thickness of 0.6 μm have been realized. The fabrication includes the processing of the mirror wafer, the processing of the electrode wafer and the assembly of the released mirror chips and diced electrode chips.[7] Fig. 5 shows a fabricated 5x5 micromirror array with flexion beam suspension. Note that the frame, to which the mirrors are suspended, runs only along one direction. The assembled device is packaged in a PGA84 housing (Fig. 6). A custom printed circuit board featuring a grid zip socket allows easy mechanical and electrical interfacing.

5. CHARACTERIZATION

Due to its location at the focal plane of the spectrograph, the surface quality of each micro-mirror must be very high, i. e. better than $\lambda/20$. In the ON position, any surface aberration will result in an image quality degradation on the detector of the spectrograph. In addition, all micro-mirrors must tilt by the same angle for optimizing the optical design of the instrument; if there is a variation in this angle, all optics have to be oversized for keeping the required performances. In the OFF position, the requirement on the mirror location is less accurate, as these mirrors send the light back toward the telescope.

A dedicated characterization bench has been developed for the complete analysis of MOEMS devices, actuators or micro-mirrors as well as full arrays. This modular Twyman-Green interferometer allows high in-plane resolution (3μm) or large field of view (40mm). Out-of-plane measurements are performed with phase-shifting

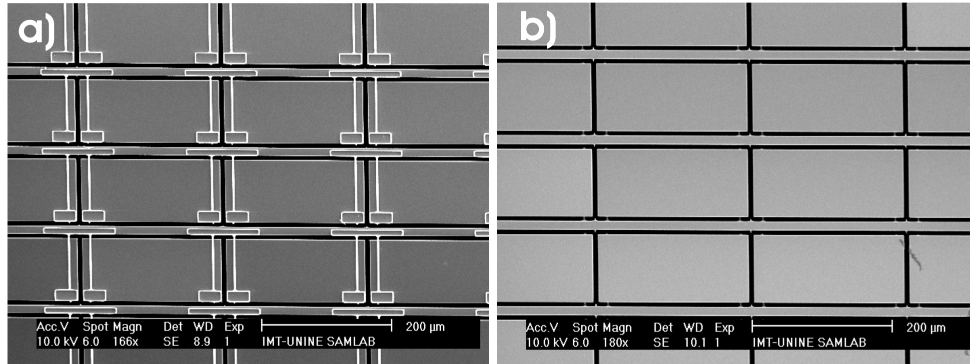

Figure 5. Fabrication Results. (a) Scanning electron microscope image of the suspension side of a microfabricated 5x5 micromirror array. The size of one mirror is 100μm x 200μm. The mirror is suspended by two cantilever flex-hinges. (b) Scanning electron microscope image of the 5x5 array showing the optical side. Note that the frame runs along only one direction, which makes possible a fill factor of 97% along the long side of the mirror.

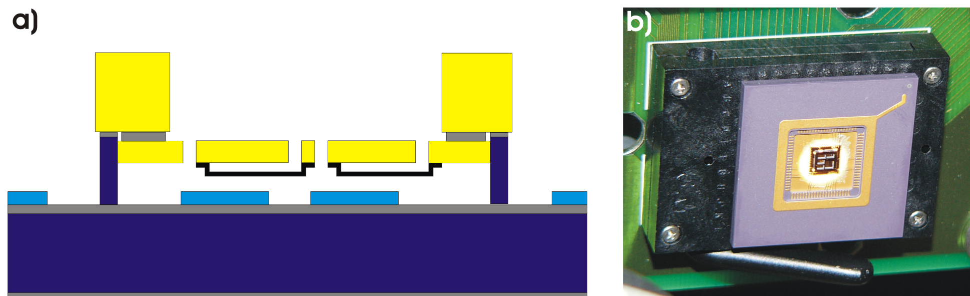

Figure 6. Assembly and packaging (a) Assembly of the mirror chip and the electrode chip. The mirror chip is put upside down on the integrated spacers of the electrode chip. The electrodes of the first run showed heights ranging from 4μm to 15μm and the spacers a height of 48μm. Within one chip the variation of the electrode height is smaller than 100nm and the variation of the spacer height smaller than 10nm. (b) Device packaged in a PGA84 housing and mounted on a custom PCB.

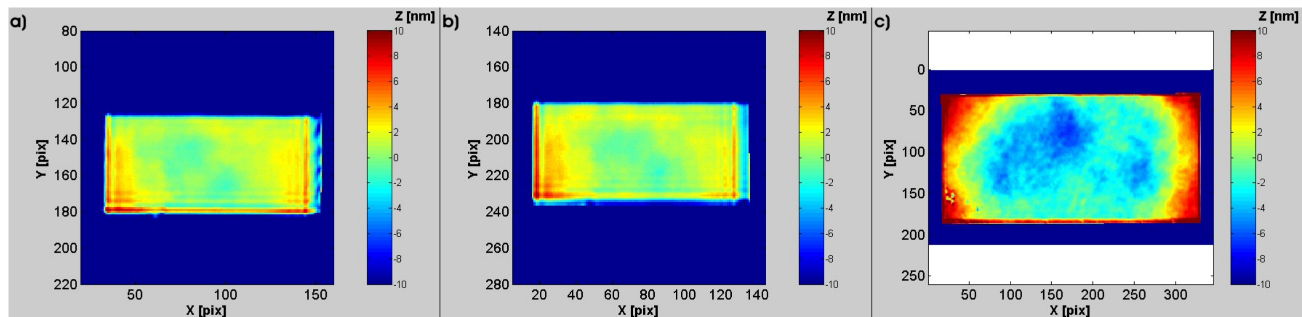

Figure 7. Surface quality of the micromirrors. Topographic images obtained from a phase shift interferometric setup (a) of a 100μm x 200μm micromirror in the OFF position (b) in the ON position and (c) of a large 250μm x 500μm micromirror in the ON state. The surface quality is not degraded when the mirror is actuated. The peak-to-valley deformation of the smaller mirrors is 8nm and 15nm in the case of the larger mirrors. The RMS roughness is around 1nm in both cases.

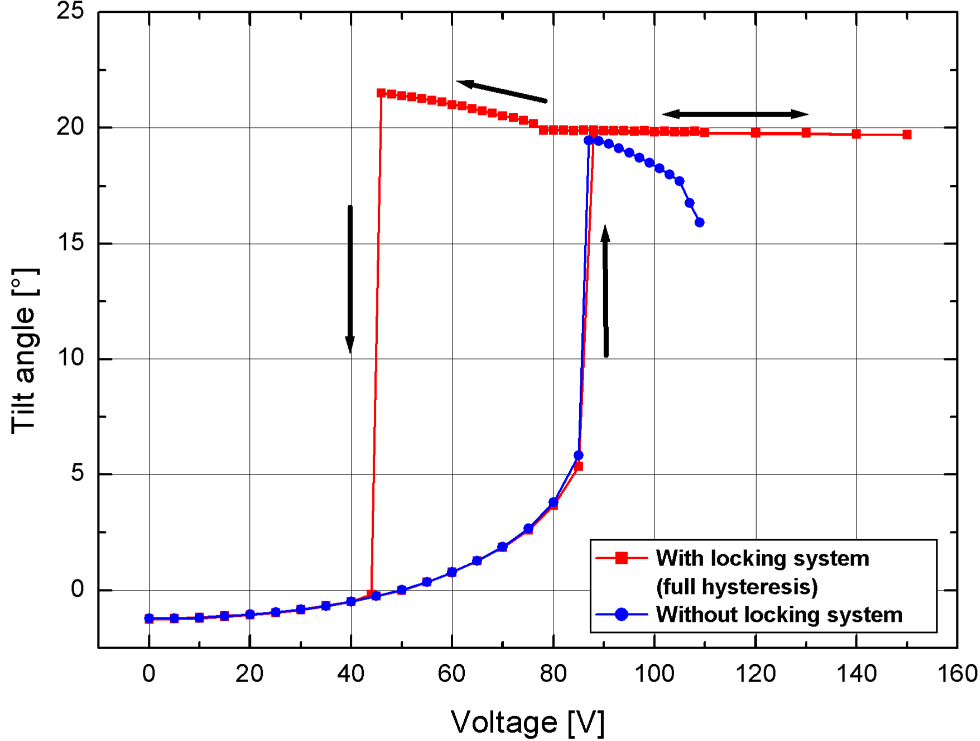

Figure 8. Tilt angle versus voltage hysteresis. The mirror with the landing beam mechanism is electromechanically latched at 20°. The angle remains stable within one arc minute over a range of 15V around the pull-in voltage.

interferometry showing very high resolution (standard deviation $<$ 1nm). Features such as optical quality or electro-mechanical behavior are extracted from these high precision three-dimensional component maps. Range is increased without loosing accuracy by using two-wavelength phase-shifting interferometry authorizing large steps measurements.[8] All measurements have been confirmed with a Veeco/Wyko NT1100 DMEMS optical profiler.

The surface quality of uncoated mirrors was measured in the OFF and the ON state. The 100μm x 200μm sized mirrors showed a peak-to-valley deformation of 7nm, in ON and in OFF position. As predicted, the mirrors remain flat when operated. The requirement on the flatness of the mirror is $\lambda/20$ for $\lambda \geq 1\mu$m, which gives 50nm. Thus our mirror quality is easily within the specifications. Larger mirrors of 250μm x 500μm, which may be used for larger telescopes, showed a PTV of 15nm, still satisfying the requirement on optical flatness. The local roughness is comparable to an unprocessed silicon wafer, which is around 1nm RMS.

The mechanical tilt angle, in function of the applied voltage, has been measured for different designs of the suspension and stopper geometry. First the applied voltage is increased until the pull-in point (at 90V) or ON state (and beyond). The tilt angle at the pull-in voltage equals the tilt angle at equilibrium, as exhibited in Section 3. From this point on, the voltage is decreased until the mirror snaps back to the OFF position. The tilt angle value at which the mirror snaps back, equals the maximum tilt angle the mirror has during the transition from the OFF to the ON state. The resulting tilt angle versus voltage hysteresis is plotted in Fig. 8, for two mirrors with $b = 20\mu$m: one mirror equipped with the stopper beams and one mirror, serving as reference, without stopper beams. We state that the maximum tilt angle and the equilibrium tilt angle are in good agreement with the simulated values (Fig. 4). Furthermore the flat region around the pull-in point of the mirror with the stopper beams proves the latching mechanism. The stopper beams hold the mirror in a stable position, precisely the tilt angle remains stable within one arcminute over a voltage range of 15V. This way process variations, which are translated into a variation of the tilt angle for a given voltage, can be suppressed. Thus the uniformity of the tilt angle over large arrays will merely depend on an uniform spacing between the micromirrors and the electrodes.

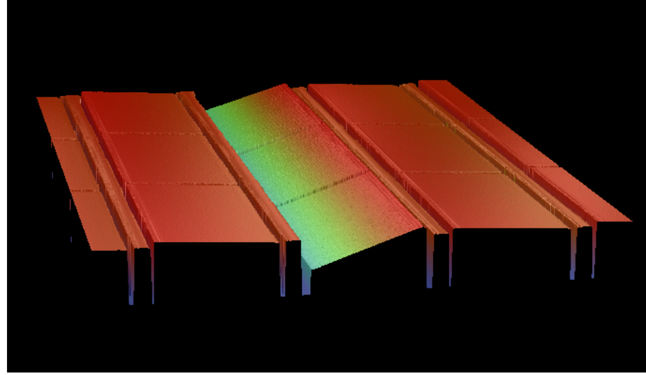

Figure 9. 3D optical profiler image of a 5x5 micromirror array. One row is actuated, implementing the long slit mode. The fill factor is 97% along the slit

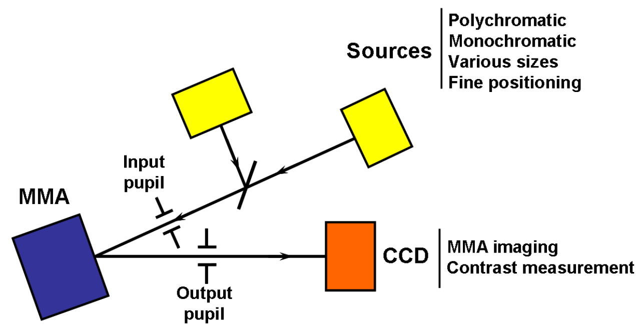

Figure 10. Object selection setup

A multicolumn system guaranteeing uniform spacing over large areas is currently under development.

We have developed a bench set-up dedicated to the operational characterization of the MOEMS-based slit masks, MMA as well as MSA, in order to be able to measure the key parameters of NIRSpec, including the contrast, defined as the ratio of the rejected light to the transmitted light. Contrast measurements have been carried out on the MMA fabricated by Texas Instrument for projection displays, in order to simulate the actual MOEMS device for NIRSpec, and to establish the test procedure.[5] We can address several parameters with our modular characterization bench, as the size of the source, its location with respect to the micro-elements, the wavelength, and the input and output pupil size. Three groups of elements are considered (Fig. 10):

- Sources: a large variety of optical sources, point or extended source, laser or white light are used. Two arms define sources by a hole or a group of holes with the proper diameter in order to simulate a typical astronomical field of view. Number of sources, relative location in the field of view, magnitude, wavelength and spectra could be chosen independently on the two arms. The sources are focused on the MMA. Fine tuning stages permit to locate very precisely the sources on the MMA. We can generate by this way the objects of interest as well as the spoiler sources.
- Component environment: injection and collection of the light to and from the MOEMS device with the possibility to configure independently the input and output pupils. According to the optical design of JWST different instruments as well as future instruments for ELTs, the optical aperture in the focal plane of the telescope could be tuned from F/6 to F/50. The output pupil of the characterization bench simulates the size of the grating inside the spectrograph. Oversizing of the output pupil is limited in a space instrument. In order to obtain high resolution images of the micro-mirrors, we are also able to use an F/2 output pupil.

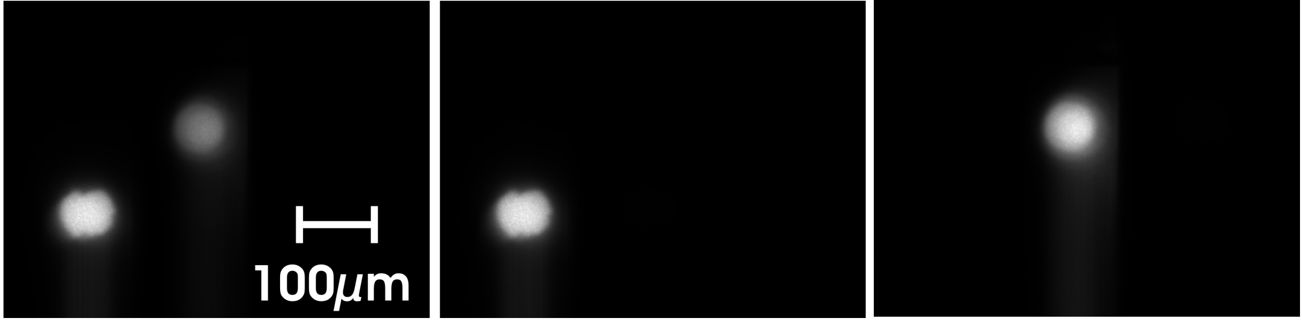

Figure 11. CCD images corresponding to the image plane of the spectrometer. In the first image, two objects are present in the field of view, in the second and third image one out of two object is selected, blocking completely the light of the other object. The projected object has a diameter of 50μm which corresponds to the size of a typical astronomical object in the focal plane of a telescope.

- Detectors: a high dynamical range CCD for device imaging and contrast measurement, and a conventional CCD for pupil imaging.

The setup was configured to demonstrate the object selection capabilities of our micromirrors. Two distinct objects are set in the field of view and a 5x5 array is used to select either one or the other object. Here the long slit mode is used, i.e. all five mirrors in a line of the 5x5 micromirror array are tilted at the same time, as illustrated in Fig. 9. Note that the fill-factor along the slit is is very high, i.e. 97%. First, both objects are selected, that is the mirror lines where the object is focussed on are tilted. Then only either the right or the left object is selected. Fig. 11 shows the series of images as seen by the CCD camera (spectrograph).

6. CONCLUSION

The presented device fulfills to a great extend the key parameters for the use in future Multi Object Spectrographs. It features optical flat mirrors that can be tilted by 20° with an actuation voltage below 100V. A system of multiple landing posts which provides uniform tilt angle has been demonstrated. The long slit mode, featuring 97% fillfactor along the slit, has been used to demonstrate object selection. To complete the demonstration, the cryogenic compatibility must be proven and larger arrays must be fabricated. The construction of a cryogenic chamber for functional testing is under way. The technology needed to fabricate large (100x200 and up) arrays of micromirror, amongst other through-wafer interconnects, is under development.

Acknowledgment

We gratefully acknowledge the COMLAB staff at the joint microfabrication facility of IMT and CSEM and Patrick Lanzoni at LAM for his valuable support during device characterization.

REFERENCES

1. F. Burg, P. Bely, B. Woodruff, J. MacKenty, M. Stiavelli, S. Casertano, C. McCreight, and A. Hoffman, "Yardstick integrated science instrument module concept for NGST," in *Proceedings of the SPIE conference on Space Telescope and Instruments V*, *Proc. SPIE* **3356**, (Kona, Hawaii), 1998.
2. F. Zamkotsian, K. Dohlen, D. Burgarella, and V. Buat, "Aspects of MMA for MOS: optical modeling and surface characterization, spectrograph optical design," in *Proceedings of the NASA conference on "NGST Science and Technology Exposition"*, *ASP Conf. Ser.* **207**, (Hyannis, USA), 1999.
3. H. Moseley, S. Aslam, M. Baylor, K. Blumenstock, R. Boucarut, A. Erwin, R. Fettig, D. Franz, T. Hadjimichael, J. Hein, A. Kutyrev, D. M. M. Li, C. Monroy, and D. Schwinger, "Microshutter arrays for the NGST NIRSpec," in *Proceedings of the SPIE conference on Astronomical Telescopes and Instrumentation 2002*, *Proc. SPIE* **4850**, (Hawaii, USA), 2002.

4. F. Zamkotsian and K. Dohlen, "Performance modeling of JWST near infrared multi-object spectrograph," in *Proceedings of the SPIE conference on Astronomical Telescopes and Instrumentation 2004*, *Proc. SPIE* **5487**, (Glasgow, United Kingdom), 2004.
5. F. Zamkotsian, J. Gautier, and P. Lanzoni, "Characterization of MOEMS devices for the instrumentation of next generation space telescope," in *Proceedings of the SPIE conference on MOEMS 2003*, *Proc. SPIE* **4980**, (San Jose, USA), 2003.
6. W. C. Young, *Roark's Formulas for Stress and Strain*, Mc Graw Hill, New York, 8th edition ed., 1989.
7. S. Waldis, P.-A. Clerc, F. Zamkotsian, M. Zickar, W. Noell, and N. F. de Rooij, "High-fill factor micro-mirror array for multi object spectroscopy," in *Proc. SPIE*, **6114**, pp. 65–76, 2006.
8. A. Liotard, S. Muratet, F. Zamkotsian, and J. Fourniols, "Static and dynamic MOEMS characterization by phase-shifting and time-averaged inteferometry," in *Proceedings of the SPIE conference on MOEMS 2005*, *Proc. SPIE* **5716**, 2005.